Article

Computational Rationalization of the Dependence of the Enantioselectivity on the Nature of the Catalyst in the Vanadium-Catalyzed Oxidation of Sulfides by Hydrogen Peroxide

David Balcells, Feliu Maseras, and Gregori Ujaque

J. Am. Chem. Soc., **2005**, 127 (10), 3624-3634• DOI: 10.1021/ja0435384 • Publication Date (Web): 19 February 2005

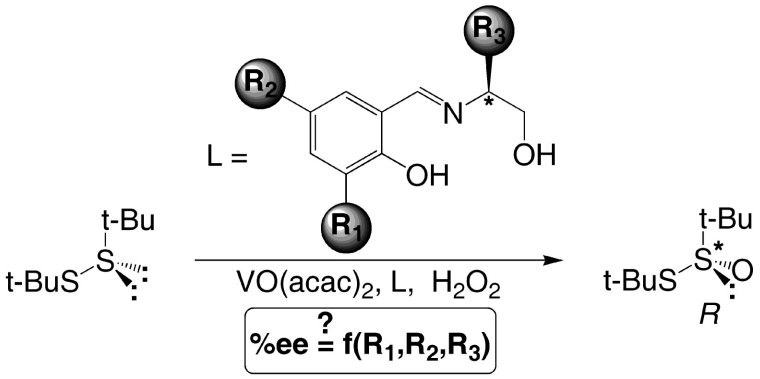

More About This Article

Additional resources and features associated with this article are available within the HTML version:

- Supporting Information
- Links to the 10 articles that cite this article, as of the time of this article download
- Access to high resolution figures
- Links to articles and content related to this article
- Copyright permission to reproduce figures and/or text from this article

View the Full Text HTML

J|A|C|S
ARTICLES
Published on Web 02/19/2005

Computational Rationalization of the Dependence of the Enantioselectivity on the Nature of the Catalyst in the Vanadium-Catalyzed Oxidation of Sulfides by Hydrogen Peroxide

David Balcells,[†,‡] Feliu Maseras,*[,†,‡] and Gregori Ujaque[‡]

Contribution from the Institute of Chemical Research of Catalonia (ICIQ), 43007 Tarragona, Catalonia, Spain; and Unitat de Química Física, Edifici Cn, Universitat Autònoma de Barcelona, 08193 Bellaterra, Catalonia, Spain

Received October 25, 2004; E-mail: fmaseras@iciq.es

Abstract: A computational study with the IMOMM(Becke3LYP:MM3) method is carried out on the mechanism of the enantioselective reaction of complex V(O)(L)(OOH), L= bulky tridentate Schiff base, and bis(*tert*-butyl) disulfide. The reaction with a given L ligand **A** is first systematically studied: different conformers of the catalyst are optimized, and the large number of associated transition states are systematically searched. The study is then extended to the geometry optimization of selected transition states associated to other ligands **B**, **C**, and **D**, similar to **A** but differing in the nature of certain substituents R_1, R_2, R_3. The experimental trends in selectivity for catalysts based on ligands **A** to **D** are faithfully reproduced by the calculations. Analysis of the computational results leads finally to the formulation of a simple model that can explain one of the most remarkable aspect of this reaction, namely the large effect on enantioselectivity of ligands seemingly far from each other in the catalyst.

Introduction

The synthesis of enantiomerically pure sulfoxides is a relevant reaction because of the direct application of these compounds as chiral auxiliaries in organic synthesis.[1−4] Several procedures have been reported for the synthesis of chiral sulfoxides,[5] and one of the most appealing is the asymmetric oxidation of prochiral sulfides,[6−23] especially in the case where an optically inactive oxidant produces the reaction with the help of a chiral catalyst. The big advantage of this procedure is that the only starting species required to be enantiomerically pure is the catalyst.

A large variety of catalytic systems involving transition metal complexes have been reported to perform the asymmetric oxidation of sulfides to sulfoxides.[9−12,15−21,24−37] Among these, the system depicted in Figure 1, from Ellman and co-workers,[15]

[†] ICIQ.
[‡] Universitat Autònoma de Barcelona.

(1) Carreño, M. C. *Chem. Rev.* **1995**, *95*, 1717.
(2) Colobert, F.; Tito, A.; Khiar, N.; Denni, D.; Medina, M. A.; Martín-Lomas, M.; Ruano, J.-L.; Solladié, G. *J. Org. Chem.* **1998**, *63*, 8918.
(3) Carreño, M. C.; Ribagorda, M.; Posner, G. H. *Angew. Chem., Int. Ed. Engl.* **2002**, *41*, 2753.
(4) Marino, J. P.; McClure, M. S.; Holub, D. P.; Comasseto, U. V.; Tucci, F. C. *J. Am. Chem. Soc.* **2002**, *124*, 1664.
(5) Fernandez, I.; Khiar, N. *Chem. Rev.* **2003**, *103*, 3651.
(6) Bolm, C.; Muñiz, K.; Hildebrand, J. P. *Comprehensive Asymmetric Catalysis*; Jacobsen, E. N., Pfaltz, A., Yamamomoto, H., Eds.; Springer-Verlag: Berlin, 1999; p. 697.
(7) Kagan, H. B. *Catalytic Asymmetric Synthesis, 2nd ed.*; Ojima, I., Ed.; Wiley-VCH: New York, 2000, p 327.
(8) Kagan, H. B.; Luukas, T. O. *Transition Metals for Organic Synthesis*, 2nd ed.; Beller, M., Bolm, C., Eds.; Wiley-VCH: Weinheim, 2004, p 479.
(9) Pitchen, P.; Deshmukh, M. N.; Duñach, E.; Kagan, H. B. *J. Am. Chem. Soc.* **1984**, *106*, 8188.
(10) Di Furia, F.; Modena, G.; Seraglia, R. *Synthesis* **1984**, 325.
(11) Nakajima, K.; Kojima, K.; Fujita, J. *Chem. Lett.* **1986**, 1483.
(12) Bolm, C.; Bienewald, F. *Angew. Chem., Int. Ed. Engl.* **1995**, *34*, 2640.
(13) Bolm, C.; Schlingloff, G.; Bienewald, F. *J. Mol. Catal. A: Chem.* **1997**, *117*, 347.
(14) Bolm, C.; Bienewald, F. *Synlett.* **1998**, 1327.
(15) Cogan, A. D.; Liu, G.; Kim, K.; Backes, B. J.; Ellman, J. A. *J. Am. Chem. Soc.* **1998**, *120*, 8011.
(16) Plitt, P.; Pritzkow, H.; Krämer, R. *Dalton Trans.* **2004**, 2314.
(17) Green, S. D.; Monti, C.; Jackson, R. F. W.; Anson, M. S.; Macdonald, S. J. F. *Chem. Commun.* **2001**, 2594.
(18) Pelotier, B.; Anson, M. S.; Campbell, I. B.; Macdonald, S. J. F.; Priem, G.; Jackson, R. F. W. *Synlett.* **2002**, 1055.
(19) Massa, A.; Siniscalchi, F. R.; Bugatti, V.; Lattanzi, A.; Scettri, A. *Tetrahedron: Asymmetry* **2002**, *13*, 1277.
(20) Capozzi, M. A. M.; Cardellicchio, C.; F., N.; Rosito, V. *J. Org. Chem.* **2002**, *67*, 7289.
(21) Smith, T. S.; Pecoraro, V. L. *Inorg. Chem.* **2002**, *41*, 6754.
(22) Schenk, W. A. *Chem. Eur. J.* **1997**, *3*, 713.
(23) Adam, W.; Korb, M. N.; Roschmann, K. J.; Saha-Moller, C. R. *J. Org. Chem.* **1998**, *63*, 3423.
(24) Saito, B.; Katsuki, T. *Tetrahedron Lett.* **2001**, *42*, 3873.
(25) Adam, W.; Malisch, W.; Roschmann, K. J.; Saha-Moller, C. R.; Schenk, W. A. *J. Organomet. Chem.* **2002**, *661*, 3.
(26) Vetter, A. H.; Berkessel, A. *Tetrahedron Lett.* **1998**, *39*, 1741.
(27) Blum, S. A.; Bergman, R. G.; Ellman, J. A. *J. Org. Chem.* **2003**, *68*, 150.
(28) Skarzewski, J.; Ostrycharz, E.; Siedlecka, R. *Tetrahedron: Asymmetry* **1999**, *10*, 3457.
(29) Skarzewski, J.; Wojazczyñska, E.; Turowska-Tyrk, I. *Tetrahedron: Asymmetry* **2002**, *13*, 369.
(30) Bryliakov, K. P.; Karpyshev, S. A.; Fominsky, A. G.; Tolstikov, A. G.; Talsi, E. P. *J. Mol. Catal. A: Chem.* **2001**, *171*, 73.
(31) Jeong, Y. C.; Choi, S.; Hwang, Y. D.; Anh, K. *Tetrahedron Lett.* **2004**, *45*, 9249.
(32) Sevvel, R.; Rajagopal, S.; Srinivasan, C.; Alhaji, N. I.; Chellamani, A. *J. Org. Chem.* **2000**, *65*, 3334.
(33) Chellamani, A.; Kylanthaipandi, P.; Rajagopal, *J. Org. Chem.* **1999**, *64*, 2232.
(34) Duboc-Toia, C.; Ménage, S.; Ho, R. Y. N.; Que, L.; Lambeaux, C.; Fontecave, M. *Inorg. Chem.* **1999**, *38*, 1261.
(35) Batigalhia, F.; Zildini-Hernandes, M.; Ferreira, A. G.; Malvestiti, I.; Cass, Q. B. *Tetrahedron* **2001**, *57*, 9669.
(36) Wang, Y.; Espenson, J. *J. Org. Chem.* **2000**, *65*, 104.
(37) Legros, J.; Bolm, C. *Angew. Chem., Int. Ed. Engl.* **2004**, *43*, 4225.

10.1021/ja0435384 CCC: $30.25

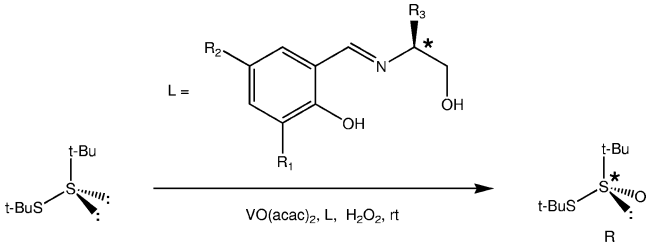

Figure 1. Vanadium-catalyzed asymmetric oxidation of 1,2-bis(*tert*-butyl)-disulfide by Ellman and co-workers.

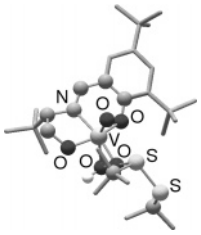

Figure 2. Definition of the QM (ball-and-stick) and MM (tube) regions in the calculation.

is quite remarkable. It applies the method originally discovered and developed by Bolm and co-workers in the mid-1990s,[12−14,38] which has been successfully used afterward by a variety of other researchers.[16,26−31] In this method, there is a precatalyst formed by a 1:1 mix of an oxo complex of vanadium (IV) and a Schiff base, and the oxidant is hydrogen peroxide. The vanadium (IV) oxo complex, introduced as $VO(acac)_2$, loses its two labile acac ligands, and produces the reactive form of the catalyst, which is a neutral vanadium (V) complex, identified by ^{51}V NMR.[12,15,30] Recent works on this same reaction system have improved its practical application.[39,40]

What makes the system in Figure 1 particularly interesting is the availability of a large body of experimental results obtained with different combinations of the R_1, R_2, and R_3 substituents in the Schiff base, and the peculiar effect of the nature of these substituents on the overall enantioselectivity of the oxidation process.[12,15] An enantiomeric excess of 82% is obtained when the three substituents are *tert*-butyl. The value is almost unchanged (83%) when R_2 is replaced by a hydrogen atom, which suggests that there is practically no effect of this substituent on the selectivity. In contrast, both R_1 and R_3 happen to be critical. Replacement of R_1 by hydrogen brings the enantiomeric excess down to 46%, while replacement of R_3 by isopropyl reduces its value to 60%. It is quite puzzling how both substituents, so far away from each other in the ligand, can have such an important effect in the overall enantioselectivity. One should expect the region of chirality to be as close as possible to the site where chemistry takes place, in a principle elegantly formulated recently by Lipkowitz and co-workers.[41] R_3 is certainly at the center of chirality in the ligand, but it is far from R_1. The ligand is furthermore quite rigid, and both substituents are thus likely to stay topologically far from each other throughout the reaction.

In this work, we present a computational study with the IMOMM method[42] on the origin of enantioselectivity in the process depicted in Figure 1. Computational chemistry has been shown to be a good complement to experiment for the elucidation of reaction mechanisms in homogeneous catalysis.[43−46] In particular, quantum mechanics/molecular mechanics (QM/MM) schemes such as IMOMM[42] and ONIOM[47] have been shown to be very efficient in the introduction of the steric effects associated to bulky ligands usually present in enantioselective catalysis.[48−54]

A previous work from our group[55] was devoted to the computational study of the reaction mechanism of disulfide oxidation on a model system where the Schiff base was HO−CH=CH−CH=N−CH_2−CH_2−OH, the disulfide was CH_3S−SCH_3 and the oxidant was HO−OH. This model system corresponded exactly to the QM region used in the QM/MM calculations presented here (Figure 2). This previous study provided the first complete picture of the reaction mechanism for the catalyzed oxidation of sulfides, thus complementing previous suggestions both from experiment[27,30] and theory,[56] and allowing to relate this chemical reaction with available computational data on epoxidation processes,[57−68] which are carried out by similar complexes. Other recent computational works on oxidation catalyzed by vanadium complexes[69−71] have focused on biomimetic models of haloperoxidases, which have somehow different structural features.[72−74]

In our study, the active catalytic species was found to be a hydroperoxo vanadium complex V(O)(L)(OOH) (L = Schiff base). The reaction takes place through a direct transfer of the oxygen group of hydroperoxo to the sulfur center, which is

(38) Bolm, C. *Coord. Chem. Rev.* **1995**, *237*, 245.
(39) Ellman, J. A.; Owens, T. D.; Tang, T. P. *Acc. Chem. Res.* **2002**, *35*, 984.
(40) Weix, D. J.; Ellman, J. A. *Org. Lett.* **2003**, *5*, 1317.
(41) Lipkowitz, K. B.; D'Hue, C. A.; Sakamoto, T.; Stack, J. N. *J. Am. Chem. Soc.* **2002**, *124*, 14255.
(42) Maseras, F.; Morokuma, K. *J. Comput. Chem.* **1995**, *16*, 1170.
(43) *Computational Modeling of Homogeneous Catalysis*; Maseras, F., Lledós, A., Eds.; Kluwer: Dordrecht, 2002.
(44) Torrent, M.; Solà, M.; Frenking, G. *Chem. Rev.* **2000**, *100*, 439.
(45) Ziegler, T. *J. Chem. Soc., Dalton Trans.* **2002**, 642.
(46) Musaev, D. G.; Morokuma, K. *Top. Catal.* **1999**, *7*, 107.
(47) Dapprich, S.; Komáromi, I.; Byun, K. S.; Morokuma, K.; Frisch, M. J. *J. Mol. Struct. (THEOCHEM)* **1999**, *461−462*, 1.
(48) Maseras, F. *Chem. Commun.* **2000**, 1821.
(49) Ujaque, G.; Maseras, F. *Struct. Bond.* **2004**, *112*, 117.
(50) Ujaque, G.; Maseras, F.; Lledós, A. *J. Am. Chem. Soc.* **1999**, *121*, 1317.
(51) Carbó, J. J.; Maseras, F.; Bo, C.; van Leeuwen, P. W. N. M. *J. Am. Chem. Soc.* **2001**, *123*, 7630.
(52) Feldgus, S.; Landis, C. R. *J. Am. Chem. Soc.* **2000**, *122*, 12714.
(53) Khoroshun, D. V.; Musaev, D. G.; Vreven, T.; Morokuma, K. *Organometallics* **2001**, *20*, 2007.
(54) Tobisch, S.; Ziegler, T. *J. Am. Chem. Soc.* **2002**, *124*, 13290.
(55) Balcells, B.; Maseras, F.; Lledós, A. *J. Org. Chem.* **2003**, *68*, 4265.
(56) Jorgensen, K. *J. Chem. Soc., Perkin Trans. 2* **1994**, 117.
(57) Rösch, N.; Di Valentin, C.; Yudanov, I. V. *Computational Modeling of Homogeneous Catalysis*; Maseras, F., Lledós, A., Eds.; Kluwer: Dordrecht, 2002, p 289.
(58) Gisdakis, P.; Antonczak, S.; Köstlmeier, S.; Herrmann, W. A.; Rösch, N. *Angew. Chem., Int. Ed. Engl.* **1998**, *37*, 2211.
(59) DiValentin, C.; Gisdakis, P.; Yudanov, I. V.; Rösch, N. *J. Org. Chem.* **2000**, *65*, 2996.
(60) DiValentin, C.; Gandolfi, P., R. Gisdakis; Rösch, N. *J. Am. Chem. Soc.* **2001**, *123*, 2365.
(61) Gisdakis, P.; Yudanov, I. V.; Rösch, N. *Inorg. Chem.* **2001**, *40*, 3755.
(62) Wu, Y. D.; Lai, D. K. W. *J. Am. Chem. Soc.* **1995**, *52*, 11327.
(63) Wu, Y. D.; Sun, J. *J. Org. Chem.* **1998**, *63*, 1752.
(64) Deubel, D. V.; Sundermeyer, J.; Frenking, G. *J. Am. Chem. Soc.* **2000**, *122*, 10101.
(65) Deubel, D. V.; Sundermeyer, J.; Frenking, G. *Org. Lett.* **2001**, *3*, 329.
(66) Deubel, D. V. *J. Phys. Chem. A* **2001**, *105*, 4765.
(67) Hroch, A.; Gemmecker, G.; Thiel, W. R. *Eur. J. Inorg. Chem.* **2000**, 1107.
(68) Sensato, F. R.; Cass, Q. B.; Longo, E.; Zuckerman-Schpector, J.; Custodio, R.; Andrés, J.; Hernandes, M. Z.; Longo, R. L. *Inorg. Chem.* **2001**, *40*, 6022.
(69) Pooransingh, N.; Pomerantseva, E.; Ebel, M.; Jantzen, S.; Rehder, D.; Polenova, T. *Inorg. Chem.* **2003**, *42*, 1256.
(70) Bühl, M.; Schurhammer, R.; Imhof, P. *J. Am. Chem. Soc.* **2004**, *126*, 3310.
(71) Zampella, G.; Kravitz, J. Y.; Webster, C. E.; Fantucci, P.; Hall, M. B.; Carlson, H. A.; Pecoraro, V. L.; Gioia, L. D. *Inorg. Chem.* **2004**, 4127.
(72) Smith II, T. S.; Pecoraro, V. L. *Inorg. Chem.* **2002**, *41*, 6754.
(73) Santoni, G.; Licini, G.; Rehder, D. *Chem. Eur. J.* **2003**, *9*, 4700.
(74) Rehder, D.; Santoni, G.; Licini, G.; Schulzke, C.; Meier, B. *Coord. Chem. Rev.* **2003**, *237*, 53.

therefore never directly attached to the metal. The breaking of the O−O bond of the oxidant and the formation of the S−O bond of the product take place simultaneously, and this process, where the oxidant acts as electrophile, is the rate-limiting step of the catalytic cycle. This is also the step where the configuration (R or S) of the product is decided, and its full understanding would thus bring that of the overall enantioselectivity. The work also showed the large conformational complexity of the system, with more than a dozen possible transition states defining near parallel paths from reactants to products.

This previous computational study[55] was however unable to tackle the issue of enantioselectivity because of the simple reason that the model Schiff base used was not chiral. The current paper overcomes this limitation by introducing the full experimental system in the calculation. In particular, the four different Schiff bases mentioned above, with different experimental selectivities associated, will be considered in the IMOMM calculations presented in what follows. The four systems will be labeled with the following arbitrary criteria based in Figure 1: **A**, with $R_1 = R_2 = R_3 = {}^t$Bu; **B**, with $R_1 = R_3 = {}^t$Bu, $R_2 = H$; **C**, with $R_1 = R_2 = {}^t$Bu, $R_3 = {}^i$Pr. and **D**, with $R_1 = R_2 = H$, $R_3 = {}^t$Bu; The fact that all R_1, R_2, R_3 substituents considered are either aliphatic alkyls or hydrogen ensures that electronic effects are approximately the same, and the differences between them must be associated to steric effects, which can be well reproduced by the IMOMM method.[75] The goal of this work is to rationalize the steric effect of the R_1, R_2, R_3 substituents (Figure 1) in the selectivity, with the hope that this can lead to the suggestion of more efficient catalysts.

Computational Details

IMOMM calculations[42] were performed with a program built from modified versions of two standard programs: Gaussian98 for the quantum mechanics part[76] and mm3(92) for the molecular mechanics part.[77] The QM region is shown in Figure 2, with $HO(CH)_3N(CH_2)_2$-OH as Schiff base and CH_3S-SCH_3 as disulfide. The rest of the system was computed at the MM level.

The QM description applied the Becke3LYP[78,79] density functional as implemented within the Gaussian98 package.[76] An effective core potential was used to replace the 10 innermost electrons of vanadium[80] and sulfur.[81] The valence double-ζ basis set associated to the pseudopotential in the program,[76] with the contraction labeled as LANL2DZ was used for these two elements, supplemented with a d shell for sulfur.[82] The 6-31G(d) basis set was used for oxygen and nitrogen,[83,84] and 6-31G for carbon and hydrogen.[83] The basis set was thus valence double-ζ for all elements, with additional polarization d shells for all atoms attached to the metal or directly involved in the oxygen transfer process.

The MM calculations were carried out with the MM3 force field.[85] van der Waals parameters for vanadium were taken from the UFF force field,[86] and torsional contributions involving dihedral angles with the metal atom in terminal position were set to zero. Besides these usual approaches, an additional modification was necessary in the MM3 force field following preliminary test calculations on the uncatalyzed reaction between bis(*tert*-butyl)disulfide and hydrogen peroxide. The proper reproduction of accurate QM CCSD(T) results required the introduction of hydrogen bond parameters between the hydrogen atoms of methyl groups and the anionic oxygen atom being transferred.[87] All geometry optimizations were full, with no restrictions except the bond distances between the QM and MM regions of the system. The frozen values were 1.400 Å for $C_{sp^2}-C_{sp^2}$, 1.550 Å for $C_{sp^3}-C_{sp^3}$ in the MM calculation; and 1.100 Å for $C_{sp^2}-H$ and 1.070 Å for $C_{sp^3}-H$ in the QM calculation.

All energies presented are potential energies in the gas phase. Enantiomeric excesses were evaluated by assuming that the relative population of products is based on the Maxwell−Boltzmann distribution of the energies of the associated transition states at a temperature of 298 K. The previous study on the model system[55] proved that relative free energies followed closely potential energies, and that extensions in the basis set and introduction of solvation effects did not affect substantially the energy profile. No frequency calculations were carried out to confirm the nature of stationary points as minima or transition states. The arrangements of the atoms at the reaction center are in all cases very similar to those calculated for the model system,[55] and in that case stationary points were indeed characterized by frequency calculations.

Results and Discussion

System with Ligand A. We will first present a detailed analysis on the case of ligand **A**, which experimentally produces a fairly high enantiomeric excess of 82%. Afterward, we will extend the study to ligands **B**, **C**, and **D**.

Catalyst. Available experimental data[12,15,27,30] had suggested that the active catalyst in this type of reactions consists of a neutral vanadium (V) oxo complex containing as ligands one peroxide unit and one Schiff base. It was not known if the ligand containing the peroxide unit was of hydroperoxo (OOH) or peroxo (OO) nature. Our previous QM calculations on a model system[55] considered four different possible isomers of the hydroperoxo complex and four more of the peroxo compound, and checked the catalytic properties of several of them. For the present QM/MM study, we will not repeat the full analysis carried on the model system. The previous study showed that the only isomer of the starting complex (**1**) relevant for catalysis was the most stable one, containing a hydroperoxo ligand. This is the only isomer of the catalyst that will be considered in the current study. Other hydroperoxo isomers in the model system differed in the orientation of the hydroxyl group of the ligand, but had energies higher by more than 4 kcal/mol. This was also the case for the peroxo isomers.

In principle, these criteria should lead to the consideration of one isomer of the catalyst, which could be labeled as **A1**,

(75) Maseras, F. *Computational Organometallic Chemistry*; Cundari, T., Ed.; Marcel Decker: New York, 2001, p 159.
(76) Frisch, M. J.; Trucks, G. W.; Schlegel, H. B.; Scuseria, G. E.; Robb, M. A.; Cheeseman, J. R.; Zakrzewski, V. G.; Montgomery, J. A., Jr.; Stratmann, R. E.; Burant, J. C.; Dapprich, S.; Millam, J. M.; Daniels, A. D.; Kudin, K. N.; Strain, M. C.; Farkas, O.; Tomasi, J.; Barone, V.; Cossi, M.; Cammi, R.; Mennucci, B.; Pomelli, C.; Adamo, C.; Clifford, S.; Ochterski, J.; Petersson, G. A.; Ayala, P. Y.; Cui, Q.; Morokuma, K.; Malick, D. K.; Rabuck, A. D.; Raghavachari, K.; Foresman, J. B.; Cioslowski, J.; Ortiz, J. V.; Stefanov, B. B.; Liu, G.; Liashenko, A. Piskorz, P.; Komaromi, I.; Gomperts, R.; Martin, R. L.; Fox, D. J.; Keith, T. Al-Laham, M. A.; Peng, C. Y.; Nanayakkara, A.; Gonzalez, C.; Challacombe, M.; Gill, P M. W.; Johnson, B.; Chen, W.; Wong, M. W.; Andres, J. L.; Gonzalez, C.; Head-Gordon, M.; Replogle, E. S.; Pople, J. A., Gaussian (Gaussian, Inc., Pittsburgh, PA, 1998).
(77) Allinger N. L, *MM3(92)*; QCPE: Bloomington, IN, 1992.
(78) Becke, A. D. *J. Chem. Phys.* **1993**, *98*, 5648.
(79) Lee, C.; Parr, R. G.; Yang, W. *Phys. Rev.* **1988**, *37*, B785.
(80) Hay, P. J.; Wadt, W. R. *J. Chem. Phys.* **1985**, *82*, 299.
(81) Wadt, W. R.; Hay, P. J. *J. Chem. Phys.* **1985**, *82*, 284.
(82) Höllwarth, A.; Böhme, M.; Dapprich, S.; Ehlers, A. W.; Gobbi, A.; Jonas, V.; Köhler, K. F.; Stegmann, R.; Veldkamp, A.; Frenking, G. *Chem. Phys. Lett.* **1993**, *208*, 237.
(83) Hehre, W. J.; Ditchfield, R.; Pople, J. A. *J. Phys. Chem.* **1972**, *56*, 2257.
(84) Hariharan, P. C.; Pople, J. A. *Theor. Chim. Acta* **1973**, *28*, 213.
(85) Allinger, N. L.; Yuh, Y. H.; Lii, J. H. *J. Am. Chem. Soc.* **1989**, *111*, 8551.
(86) Rappé, A. K.; Casewit, C. J.; Colwell, D. S.; Goddard, W. A.; Skiff, W. N. *J. Am. Chem. Soc.* **1992**, *114*, 10024.
(87) Balcells, D.; Drudis-Solé, G.; Besora, M.; Dölker, N.; Ujaque, G.; Maseras, F.; Lledós, A. *Faraday Discuss.* **2003**, *124*, 429.

Table 1. Selected Optimized IMOMM(Becke3LYP:MM3) Geometrical Parameters (Å and Degrees) of the More Stable Isomeric Forms of the Catalyst[a]

	model	A1aa	A1as	A1ba	A1ba′	A1bs	A1bs′
V−O2	1.811	1.812	1.812	1.822	1.816	1.823	1.817
O2−O3	1.449	1.449	1.449	1.450	1.451	1.450	1.452
V−O2−O3	95.8	96.5	96.6	95.0	94.2	94.8	94.0
O5−V−O2−O3	66.7	67.5	67.3	−68.2	−67.8	−68.6	−68.3
C1−C2−C3−C4		179.8	0.7	178.4	178.2	−0.2	1.2
N−V−O5−C8	−32.1	−29.2	−29.1	−14.0	44.5	−13.6	44.6
energy	0.0	0.0	1.1	1.9	2.2	2.9	3.2

[a] The relative potential energy in kcal/mol is relative to isomer **A1aa**.

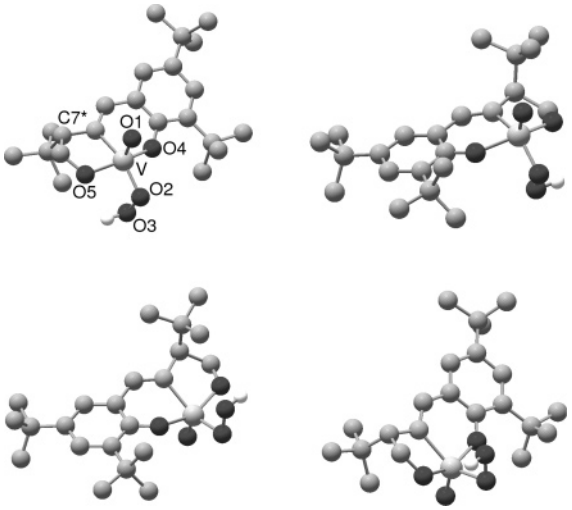

Figure 3. Two different views of diastereomers **A1a** (left) and **A1b** (right) of the catalyst.

where **A** would correspond to the **A** ligand used in the catalyst, and **1** would be the label associated to the catalyst molecule in the catalytic cycle. Unfortunately, things are more complicated. The consideration of the full system in the calculations introduces sources of isomeric complexity that were absent in the simplified model system. Table 1 presents geometrical parameters for six different isomeric forms of the catalyst, as well as for the model system with the simplified ligand $O(CH)_3N(CH)_2O$. All structures have a similar arrangement, as shown by the very similar values of the V−O2 and O2−O3 distances, the V−O2−O3 angle, and the O5−V−O2−O3 dihedral angle (see Figure 3 for labeling). In what follows, we will analyze why there are so many different isomers with this same structural motif at the reaction center.

The main complication when considering the real ligands instead of the simplified model system is the existence of two diasteromeric forms of the catalyst. Their presence requires the introduction of an additional letter in the labeling, resulting in the existence of structures such as **A1a** and **A1b**. Two different views of the optimized IMOMM(Becke3LYP:MM3) geometries of **A1a** and **A1b** are shown in Figure 3. The diastereomerism arises from the presence of two chiral centers in the catalyst molecule. One of them is the carbon atom C7 in the five-member ring where substituent R_3 is attached. The chirality of this center is defined by the enantiopure reactive being used experimentally. The second chiral center is the vanadium atom. This chiral center is formed in the reaction media, when the chelating ligand binds to vanadium. The combination of both chiral centers could give rise to four possible configurations, two diastereomers and their corresponding enantiomers. The enantiomers are not available because of the enantiopure form of the ligand being used, and

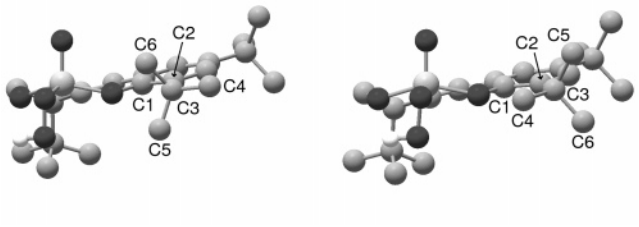

Figure 4. Conformations **A1aa** (left) and **A1as** (right) of the catalyst.

the two diastereomers are shown in Figure 3. According to this, the labels need to be extended to differentiate these new structures. Hence, the structures shown in Figure 3 are labeled **A1a** and **A1b**, respectively. In molecule **A1a** *tert*-butyl R_3 is in the face opposite to the oxo ligand; while in molecule **A1b**, both the oxo group and R_3 are in the same side of the five-member ring. Diastereomer **A1a** is 1.9 kcal/mol more stable than diastereomer **A1b**. Both possible forms of the catalyst will be considered in the following subsections.

The presence of bulky substituents in the full catalyst also leads to the appearance of different stable conformers. In particular, the two shown in Figure 4 differ only in the orientation of the *tert*-butyl substituent R_1 attached to C2. The structure on the left corresponds to the geometry already shown in Figure 3 that had been labeled as **A1a**. In this conformer, one of the methyl substituents of *tert*-butyl R_1 (C4) lies approximately in the phenyl plane anti with respect to carbon C1; its complete label is **A1aa**. In the structure on the right of Figure 4, the C4 substituent of R_1 is syn with respect to C1; this conformer is thus labeled **A1as**. The energy of **A1aa** is 1.1 kcal/mol below that of **A1as**. A similar set of conformations exists for the diastereomeric form of the catalyst, **A1b**, which produces conformers **A1ba** and **A1bs**, 1.9 and 2.9 kcal/mol above **A1aa**, respectively. The relationship between the **A1aa**/**A1as** and **A1ba**/**A1bs** can be clearly seen in Table 1, where they differ in practice only in the value of the C1−C2−C3−C4 dihedral angle, associated to the rotation of this particular *tert*-butyl group. R_1 is relatively close to the hydroperoxo group, in the region where the reaction takes place, and therefore both of these **a** and **s** conformers have to be considered in the mechanistic study. Only the two conformers just described were found to be associated to the rotation of R_1. The arrangement of R_2 may also give rise to different conformers of **A1**, but being the modifications further away from the reaction center, these species were not considered, and we just made sure that the arrangement was the same in all computed structures. The case of the substituent R_3 is more simple, because it is attached to a sp^3 carbon and takes the expected staggered conformation.

A last source of flexibility in the catalyst, which was already present in the model system,[55] but that is magnified by the

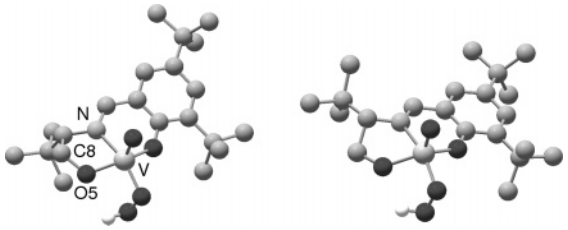

Figure 5. Conformations **A1aa** (left) and **A1aa′** (right) of the catalyst.

introduction of the real substituents, concerns the arrangement of the five-member ring. This ring has the expected envelope shape analogous to that observed in cyclopentane, and two stable conformations can be optimized for each of the structures reported above. Figure 5 presents, as an example, isomers **A1aa** and **A1aa′**, the latter being 6.3 kcal/mol above the former. For consistence with the labeling used on the model systems, the second isomer of this type will always be indicated with the ' sign. It can also be seen in Table 1 that the values for the N−V−O5−C8 dihedral angle, which characterize this isomer, are much less systematic than in the case of the other geometrical changes considered, with values around −29°, −14°, and 44°. Isomers **A1aa′** and **A1as**' are not included in the Table because of their higher energy (6.3 and 7.4 kcal/mol above **A1aa**, respectively). Their corresponding values for this dihedral angle, −3.1° and −7.0°, respectively, add to the dispersion observed for the value of this dihedral angle.

In summary, we can see that even after the definition of a given ligand, **A**, and a given arrangement of the hydroperoxo ligand in the catalyst **1**, there are still eight possible structures that can be considered, depending on the choice of: (i) diastereomeric form of the catalyst (**a** or **b**), (ii) arrangement of the *tert*-butyl R_1 (**a** or **s**); and (iii) conformation of the envelope-shaped five-membered ring (′ or not). According to this labeling, the 8 isomers are **A1aa**, **A1aa′**, **A1as**, **A1as′**, **A1ba**, **A1ba′**, **A1bs**, and **A1bs′**. Their relative energies are 0.0, 6.3, 1.1, 7.4, 1.9, 2.2, 2.9, and 3.2 kcal/mol, respectively. Some of the structures have been presented in Figures 3 to 5, selected geometrical parameters of the six more stable structures are collected in Table 1, and the Cartesian coordinates of all of them are given in the Supporting Information. To our knowledge, no detailed experimental information is available on which is the most stable form of the catalyst, and one has to assume that, in principle, several of them can coexist in equilibrium.

Transition States Associated to the Diastereomeric Form A1a. The computational estimation of the enantiomeric excess will of course be associated to the relative energy of the transition states of the reaction step where the enantioselectivity is decided. The nature of this step was well characterized in our previous study of the reaction on a small model system.[55] Let us summarize here briefly the more relevant results from that work concerning this reaction step. It is a direct transfer process, where an oxygen atom of the OOH group is "transferred" to the disulfide without coordination of the latter to the metal center. In this transition state, the disulfide binds to the oxygen atom O2 (see Figure 3), that initially attached to the metal. The possibility of attack to the other hydrogen, O3, was also examined, but no transition states could be located. Examination of NPA and Mulliken charges indicated that the reaction is an electrophilic attack of the hydroperoxo moiety on the sulfur center. This is in fact consistent with the near linear

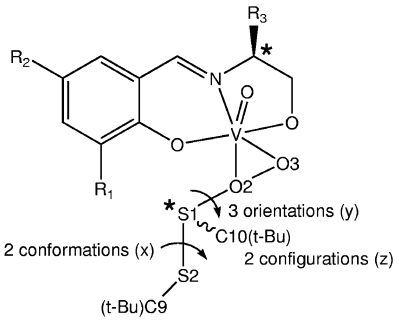

Figure 6. Sources of conformational flexibility in structures **A2a**.

arrangement of the S−O−O group, indicating the essential role played by the O−O σ^* orbital in the interaction.[88] The result of this reaction step is a complex, where an OH group is attached to the metal. This species can react afterward with hydrogen peroxide to regenerate the starting complex and produce water as subproduct. The free energy barrier for this key transition state on the model system was found to be 26.7 kcal/mol above reactants, well below the 40.4 kcal/mol associated to the uncatalyzed reaction.

In principle, the transition states connected to all the isomers of the catalyst presented above should be computed. For the sake of simplicity, the analysis of these transition states is divided in two parts, depending on the diastereomeric form of the catalyst being considered. In this subsection, the results correspond to the consideration of structures associated to the diastereomeric form **A1a**. Following the scheme presented above, this would correspond to transition states associated to the catalyst isomers **A1aa**, **A1aa′**, **A1as**, and **A1as′**. The energies of the isomers **A1aa′**, **A1as′** are quite high above that of **A1aa**, 6.3 and 7.4 kcal/mol, respectively, and because of that, these isomers are directly discarded.

The previous study on the model system[55] also showed that the transition state has a remarkable flexibility, with several geometrical features that can be modified to produce similar structures able to connect reactants to products. These sources of conformational flexibility, all of them related to the way in which the disulfide substrate approaches the catalyst, are summarized in Figure 6. The study on the model system also identified the reasonable values for the dihedral angles characterizing each of these possible geometrical variations. For the O2−S1−S2−C9 torsion (labeled as **x**), associated to the conformation of the bis(*tert*-butyl) disulfide substrate, starting values for the geometry optimization are −30° and 170°, giving rise to labels **x1** and **x2**. For the V−O2−S1−S2 dihedral angle (**y**), related to the orientation of the substrate with respect to the catalyst, possible starting values are 180° (**y1**), −90° (**y2**), and 50° (**y3**). Finally, the dihedral angle C10−S1−S2−O2, characterizing the critical absolute configuration of S1, has possible starting values of 120° (**z1**) and −120° (**z2**). Transition states were systematically searched in the model system with the different **xyz** combinations. For most of them close energies were found, within a span of 2 kcal/mol, with the sole exception of option **y3**, which was associated in all cases to higher energy transition states.

The study here performed is analogous to that carried out on the model system. As mentioned above, there are two low

(88) Bach, R. D.; Wolber, G. J.; Coddens, B. A. *J. Am. Chem. Soc.* **1984**, *106*, 6098.

Table 2. Selected Optimized IMOMM(Becke3LYP:MM3) Geometrical Parameters (Å and Degrees) and Energies of the Six Lower Energy Transition States A2a Associated to the Diastereomeric Form A1a of the Catalyst[a]

	ax1y1z1	ax2y2z1	sx2y2z1	ax1y1z2	sx1y1z1	sx1y1z2
O2−S1	2.099	2.088	2.104	2.112	2.097	2.120
O2−O3	1.850	1.845	1.839	1.853	1.850	1.845
O2−S1−S2−C9 **(x)**	0.6	138.4	141.4	−11.2	−4.9	−11.0
V−O2−S1−S2 **(y)**	−163.0	−77.4	−85.6	151.9	−168.3	151.7
C10−S1−S2−O2 **(z)**	106.7	93.4	92.0	−100.4	111.7	−101.8
energy	0.0	1.3	1.8	2.4	2.5	2.5

[a] The potential energy in kcal/mol is relative to that of **A2aax1y1z1**.

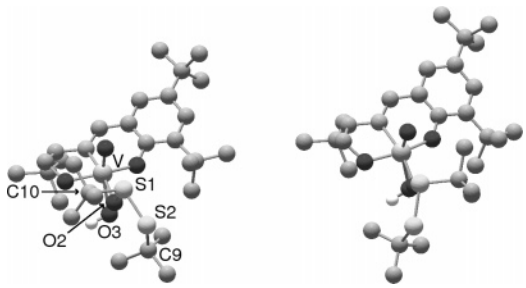

Figure 7. Transition states **A2aax1y1z1** (left) and **A2aax1y1z2** (right).

energy isomeric forms of the **A1a** diastereomer, namely **A1aa** and **A1as**. For everyone of them, eight possible transition states were searched, corresponding to the existence of three dihedral angles with two possible values each of them. Unlike the model system, calculations corresponding to the third possible value for the second dihedral angle V−O2−S1−S2, with the associated label **y3**, were not explicitly carried out because the starting geometry was sterically very hindered, in agreement in fact with the relatively high energy of this conformation in the model system. Therefore, a total of sixteen IMOMM calculations were launched. The labels for the transition states were systematically defined by replacing the number **1** by **2** in the label of the corresponding catalyst structure, and adding the **xyz** labels corresponding to the actual conformation. Thus, labels such as **A2aax1y1z1** are obtained. Not all of these sixteeen calculations converged to distinct transition states, but twelve of them did. Two of the failed calculations collapsed to other transition states, while the other two reverted to reactants. Selected geometrical parameters of the six lower energy transition states, as well as their relative energies, are collected in Table 2. It can be seen that the values for the main two bonds being formed and broken, O2−S1 and O2−O3, are very similar between them, with values around 2.10 Å for the former, and around 1.84 Å for the latter. These values are moreover close to those reported for the model system, furthermore confirming the nature of these structures as transition states for the process under study. The optimized values for the dihedral angles **x**, **y**, **z** reported in Table 2 are reasonably close to their starting values (see above).

The most significant results from Table 2 are the relative energies. The lowest energy transition state is **A2aax1y1z1**, which leads to the **R** product, a result that is in agreement with the experimental observation. This structure is shown in Figure 7. It is worth mentioning that it has the same **x1y1z1** arrangement preferred also in the model system.[55] Apart from this coincidence, differences are significative, further confirming the need for full QM/MM optimizations. The second most stable structure for the model system was **x1y1z2**, only 0.8 kcal/mol above the lowest energy transition state. Now the corresponding structure, **A2aax1y1z2**, is the fourth more stable structure, 2.4 kcal/mol above the lowest one. This is a significant energy difference, because **A2aax1y1z2**, despite being only the fourth in the energy order, is the lowest one with the **z2** label, indicative of structures going to the **S** product. The energy separation between transition states leading to different enantiomers is critical for enantiomeric excess, and this is a first computational indication of the effect of bulky substituents on it.

Examination of Table 2 shows that four of the structures have the **z1** label, associated to the **R** product, and two of them have the **z2** label, associated to the **S** product. Figure 7 shows the structure of the lowest energy transition states leading to the **R** and **S** products, **A2aax1y1z1** and **A2aax1y1z2**, respectively. Comparison between them is quite simple, since they differ only in the **z** label, the configuration around chiral center S1. In the drawing it can be seen that carbon C10 goes left from the S1 center for the **z1** isomer, and it goes toward the right for the **z2** isomer. In this latter isomer, this C10 *tert*-butyl has a certain steric repulsion with the *tert*-butyl substituent in the R_1 position, which is relatively close. The fact that the difference between both structures is mainly steric is further confirmed by the partition of the total QM/MM energy in its contributions. The total energy difference of 2.4 kcal/mol between **A2aax1y1z2** and **A2aax1y1z2** comes from 0.5 kcal/mol in the QM term and 1.9 kcal/mol in the MM term.

From the energy difference between the most stable transition states leading to each of the enantiomers one can make an estimation of the enantiomeric excess. The idea is to assume that all the **R** product comes from one transition state, and all the **S** product comes from the other one. The result would be more accurate if all the possible transition states were put in the equation but, as will be shown below, systematic consideration of all possible transition states is practically impossible, and with this first approach we can have an estimation of the expected enantiomeric excess. With this assumption, and considering that the population of products is proportional to the Boltzmann distribution of transition state energies, an energy difference of 2.4 kcal/mol leads to an enantiomeric excess of 97% for the **R** product at 298 K. This is certainly much larger than the experimental observation of 82%, but the result has to be refined by taking into account the contribution from the second diastereomeric form of the catalyst.

Transition States Associated to the Diastereomeric form A1b. The catalytic properties of the second diastereomeric form of the catalyst **A1b**, which must be in equilibrium in solution with **A1a**, are analyzed here. The study of **A1b** is in principle more complicated because of the presence of four close energy conformations for the catalyst, **A1ba**, **A1ba′**, **A1bs**, **A1bs′**, in contrast with the two that were available for **A1a** (Table 1). Because of this, we will simplify the study of **A1b** by extrapolating some of the conclusions previously obtained. In

Table 3. Selected Optimized IMOMM(Becke3LYP:MM3) Geometrical Parameters (Å and degrees) and Energies of the Five Optimized Transition States A2b Associated to the Diastereomeric Form A1b of the Catalyst[a]

	sx1y1z2	ax1y1z1	sx1y1z2′	ax1y1z1′	ax1y1z2′
O2−S1	2.119	2.138	2.099	2.123	2.088
O2−O3	1.837	1.847	1.855	1.855	1.860
O2−S1−S2−C9 **(x)**	0.4	7.0	0.7	9.2	7.9
V−O2−S1−S2 **(y)**	164.4	−155.5	163.9	−158.0	169.8
C10−S1−S2−O2 **(z)**	−107.5	108.7	−107.7	106.4	−114.0
energy	1.8	3.6	3.0	3.0	3.3

[a] The potential energy in kcal/mol is relative to that of **A2aax1y1z1**.

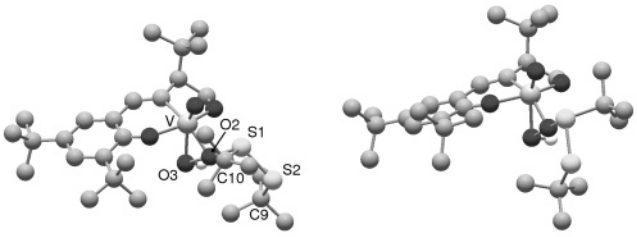

Figure 8. Transition states **A2bax1y1z1** (left) and **A2bsx1y1z2** (right).

particular, we will assume that the most stable conformation of the dihedral angles O2−S1−S2−C9 and V−O2−S1−S2 is always that corresponding to the **x1y1** labels. In the case of **A1a**, this was the arrangement for the most stable transition states leading to either the **R** or the **S** products.

Two structures (**z1** and **z2**) were considered for each of the four conformations of the catalyst **A1b**. As a result, eight IMOMM calculations were launched. Five of them converged to distinct transition states. Table 3 collects their selected geometric parameters and relative energies. The values for the O2−S1 and O2−O3 distances are similar for the different structures, as well as with those of Table 2, further proving that these structures indeed correspond to transition states of the process of oxidation of the disulfide. The **x** values are in all cases close to 0°, while the **y** values cluster around 180°, indicating that the labeling of the conformations is correct. The presence of **z1** and **z2** labels at relatively similar energies indicates that both the **R** and **S** products can be in principle also obtained from this diastereomeric form of the catalyst.

The relative energies are again the most relevant result from these calculations. The lowest energy transition state of the five presented in Table 3 is **A2bsx1y1z2**, with a relative energy of 1.8 kcal/mol above **A2aax1y1z1**. This is clearly the most stable of the five structures, with the following ones, **A2bsx1y1z2′** and **A2bax1y1z1′**, having relative energies of 3.0 kcal/mol. It is worth remarking that the most stable geometry **A2bsx1y1z2** has a **z2** label, indicating that it leads to the **S** product. This is in sharp contrast to what happened in the case of the **A1a** form of the catalyst, which was pro-**R**. The reasons can be understood by looking at Figure 8, where the geometries of transition states **A2bax1y1z1** and **A2bsx1y1z2** are shown. In this case, the **z2** structure is the less sterically hindered, because the ^{t}Bu substituent at S1 is pointing toward a free space, while in the **z1** structure is pointing toward the ^{t}Bu substituent R_1. The situation is completely opposite to that of the **a** form of the catalyst, previously shown in Figure 7. This behavior can be in fact traced down to the chirally opposite arrangement of substituents at the vanadium chiral center, which marks in fact the difference between the two diastereomeric forms of the catalyst.

In contrast with the structures derived from **A1ba** and **A1bs**, which show a clear energy difference of 1.8 kcal/mol between pro-**S** and pro-**R** transition states, those deriving from **A1ba′** and **A1bs′** are practically degenerate, with a difference of less than 0.1 kcal/mol between **A2bsx1y1z2′** and **A2bax1y1z1′**. Because of their small selectivity, and because they contribute very little to the overall outcome of the reaction, this type of structures will be neglected in the rest of the paper.

The fact that the **A1b** form of the catalyst is pro-**S** is interesting, but has no direct bearing to the experimental observations because the **a** and **b** forms of the catalyst are not isolated. What is important from the experimental point of view is wheather the transition states coming from **A1b** can compete with those coming from the lower energy catalyst forms **A1a**. The contribution from **A1b** to the **R** product is certainly small, with the lowest energy **b** transition state **A2bax1yz1′** 3.0 kcal/mol above the lowest **a** transition state **A2aax1y1z1**. But things are very different for the **S** product. Structure **A2bsx1y1z2** is in fact 0.6 kcal/mol below **A2aax1y1z2**, indicating that the main part of **S** product comes from the **b** form of the catalyst. Therefore, the estimation of the enantiomeric excess presented in the previous section has to be recalculated taking into account this new result. This energy difference of 1.8 kcal/mol between transition states leading to the **R** and **S** products corresponds to an enantiomeric excess of 90%. It is still higher than the experimentally measured value of 82%, but it is a substantial improvement from the 97% that had been computed above. It is in any case clear that both diastereomeric forms of the catalyst have to be taken into account to compute the overall selectivity, because each enantiomer of the product comes mainly from a different form of the catalyst.

Systems with Ligands B, C, and D. This section presents our computational results on ligands **B**, **C** and **D**, which present different combinations of R_1, R_2, R_3 substituents (Figure 1) than ligand **A**, resulting in different experimental enantiomeric exccesses. Although, in principle, each new ligand could be analyzed with the systematic approach described above for ligand **A**, we will assume here that the energetic ordering of the structures follows a similar pattern and will compute only some selected transition states. This is reasonable because of the high similarity of the compounds, and the result will furthermore be checked by comparing the computed enantioselectivity with the experimental value.

The previous analysis has shown the importance of the existence of two diastereomers of the catalyst. In consequence, both of them will be taken into account. Each of these diastereomeric forms of the catalyst is associated to a variety of transition state geometries. The most significant ones for the evaluation of the enantiomeric excess are the most stable structures leading to each of the enantiomeric products, **R** and

Table 4. Relative Energies (kcal/mol) of the Four Selected Transition States Computed for Each of the Possible Ligands A, B, C, and D[a]

	A	B	C	D
2aax1y1z1	0.0	0.0	0.0	0.0
2aax1y1z2	2.4	2.4	2.7	0.3
2bsx1y1z2	1.8	1.8	1.1	0.3
2bax1y1z1	3.6	3.3	1.9	0.7
computed ee	90	90	74	21
experimental ee	82	83	60	46

[a] The resulting computed enantiomeric excess, as well as the experimental value, are also provided.

Table 5. Selected Optimized IMOMM(Becke3LYP:MM3) Geometrical Parameters (Å and Degrees) and Energies of the Four Computed Transition States B2 Associated to the B Ligand[a]

	aax1y1z1	aax1y1z2	bsx1y1z2	bax1y1z1
O2−S1	2.099	2.112	2.119	2.140
O2−O3	1.850	1.853	1.836	1.842
O2−S1−S2−C9 **(x)**	0.5	−11.0	0.6	7.0
V−O2−S1−S2 **(y)**	−162.9	151.7	164.6	−148.4
C10−S1−S2−O2 **(z)**	106.7	−100.5	−107.7	106.5
energy	0.0	2.4	1.8	3.3

[a] The potential energy in kcal/mol is relative to that of **B2aax1y1z1**.

S. Because of this, only two geometries will be taken for each diastereomeric form. Therefore, four transition states will be computed for each new ligand, corresponding to the labels **2aax1y1z1**, **2aax1y1z2**, **2bsx1y1z2**, and **2bax1y1z1**, according to the results presented above for ligand **A**. The relative energies of all these sixteen computed structures are collected in Table 4.

Ligand **B** has $R_1 = R_3 = {}^t$Bu, $R_2 =$ H, it thus differs from **A** only in the R_2 substituent, which was also ^{t}Bu in the latter. The experimental enantiomeric excess associated to both ligands is practically the same, 82% for **A** and 83% for **B**. Table 5 collects the relative energies and selected geometrical parameters of transition states **B2aax1y1z1**, **B2aax1y1z2**, **B2bsx1y1z2**, and **B2bax1y1z1**. From Tables 2 to 5, it can be seen that both the selected geometrical parameters and the relative energies of these four structures are practically the same as those computed for ligand **A**. The relative energies (Table 4) are identical to the tenth of kcal/mol, with the only exception of the least stable structure **B2bax1y1z1**, which presents a small difference of 0.3 kcal/mol (3.6 vs 3.3). As a result, the computed enantiomeric excess is exactly the same, 90%, for both ligands. The computational prediction of an identical enantiomeric excess fits very well with the experimental observation of a difference of only 1%. The interpretation of the result is furthermore straightforward. Substituent R_2 is far away from the reaction center, as could already be observed in Figures 7 and 8 for ligand **A**, and the nature of R_2 has no effect on the outcome of the reaction. This result is in no contradiction with the experimentally well documented effect of R_2 on the reaction for other systems different from those considered here. Enantiomeric excess is indeed affected when R_2 is replaced by NO_2,[12] or I.[18] The explanation is that in these two particular cases the substituents have important electronic effects. These cannot be taken into account by an IMOMM calculation with the QM/MM partition used in this work, but should be in principle reproduced if the NO_2 and I groups were introduced in the QM region.

Table 6. Selected Optimized IMOMM(Becke3LYP:MM3) Geometrical Parameters (Å and Degrees) and Energies of the Four Computed Transition States C2 Associated to the C Ligand[a]

	aax1y1z1	aax1y1z2	bsx1y1z2	bax1y1z1
O2−S1	2.100	2.110	2.114	2.130
O2−O3	1.856	1.858	1.841	1.851
O2−S1−S2−C9 **(x)**	2.2	−10.5	1.3	8.5
V−O2−S1−S2 **(y)**	−162.6	152.6	165.2	−155.8
C10−S1−S2−O2 **(z)**	105.9	−100.9	−108.4	106.5
energy	0.0	2.7	1.1	1.9

[a] The potential energy in kcal/mol is relative to that of **C2aax1y1z1**.

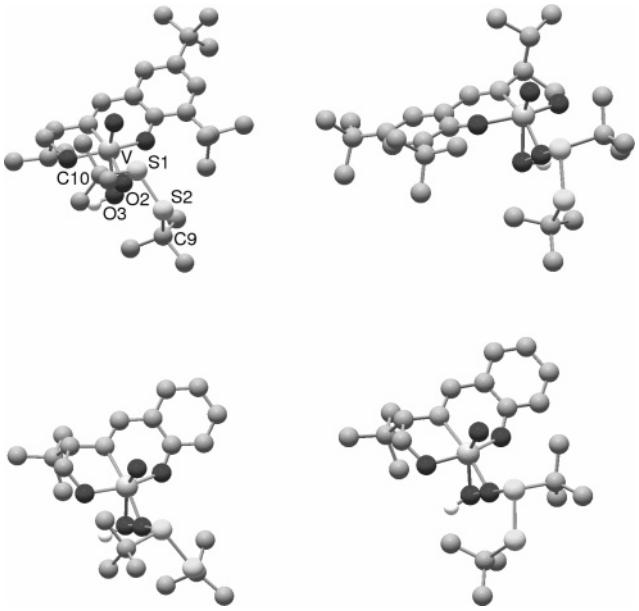

Figure 9. Transition states **C2aax1y1z1** (upper left), **C2bsx1y1z2** (upper right), **D2ax1y1z1** (lower left), and **D2ax1y1z2** (lower right).

Ligand **C** has $R_1 = R_2 = {}^t$Bu, $R_3 = {}^i$Pr, it differs from **A** thus on the nature of R_3, which in this case is ^{i}Pr instead of ^{t}Bu. This change implies a reduction in the enantiomeric excess of the product, which drops from 82% to 60%. Table 6 contains relative energies and selected geometrical parameters of the computed transition states **C2aax1y1z1**, **C2aax1y1z2**, **C2bsx1y1z2**, and **C2bax1y1z1**, and the two most stable among them are shown in Figure 9. Differences in geometrical parameters between species associated to **A** and to **C** are quite small, albeit more important than those between **A** and **B**. Comparison of relative energies (Table 4) is more interesting. In the case of **C**, the lowest energy transition state leading to the **S** isomer, **C2bsx1y1z2**, has an energy of only 1.1 kcal/mol above the most stable transition state overall, **C2aax1y1z1**, which leads to the **R** isomer. This energy difference translates into a computed enantiomeric excess of 74%, clearly lower than that computed for **A**, 90%. The fact that the enantiomeric excess for **C** is smaller than that for **A** reproduces again the experimental observation.

It must be mentioned here that the presence of ^{i}Pr in the R_3 position introduces an additional source of conformational complexity, since the three staggered positions available for the two methyl and one hydrogen substituents of ^{i}Pr are not equivalent. However, the solution is in this case simple, the hydrogen occupies always the most hindered position, toward the center of the five-member ring, as shown in the structures in Figure 9. We confirmed this result by computing the two

Table 7. Selected Optimized IMOMM(Becke3LYP:MM3) Geometrical Parameters (Å and Degrees) and Energies of the Four Computed Transition States D2 Associated to the D Ligand[a]

	ax1y1z1	ax1y1z2	bx1y1z2	bx1y1z1
O2−S1	2.098	2.099	2.121	2.121
O2−O3	1.858	1.860	1.844	1.847
O2−S1−S2−C9 **(x)**	15.9	−14.4	−13.4	14.0
V−O2−S1−S2 **(y)**	−153.4	156.5	146.5	−155.0
C10−S1−S2−O2 **(z)**	97.9	−97.5	−99.4	98.1
energy	0.0	0.3	0.3	0.7

[a] The potential energy in kcal/mol is relative to that of **D2ax1y1z1**.

alternative rotamers for each of the two structures in the Figure. The conformational variations of **C2aax1y1z1** had energies 0.8 and 2.6 kcal/mol above, and the corresponding values for the conformational variations of **C2bsx1y1z2** were 1.8 and 3.3 kcal/mol above.

The crucial reduction of the energy difference between the two key transition states for ligand **C** is part in fact of the general trend of reduction of the energy difference between structures coming from diastereomers **a** and **b** of the catalyst. **C2aax1y1z1** is still the most stable structure, but **C2bsx1y1z2** and **C2bax1yz1** are only 1.1 and 1.9 kcal/mol above, while the corresponding values for **A** were 1.8 and 3.6 kcal/mol, respectively. In contrast, the effect is not so clear for the relative energies coming from the same diastereomeric form, with the difference between **C2aax1y1z1** and **C2aax1y1z2** being actually larger than for the corresponding **A** systems (2.7 vs 2.4 kcal/mol). The replacement of the R_3 substituent affects therefore the relative energy of the two diastereomers of the catalyst, and this affects the overall enantioselectivity because each isomer comes from a different catalytic form. If we could isolate the **C2a** form of the catalyst and perform the reaction exclusively with it, the enantioselectivity would be much higher.

The mechanism by which R_3 affects the stability of the diastereomeric forms of the catalyst is quite straightforward. In fact, R_3 is attached to the only chiral center of the ligand, C7 (see Figure 3). If R_3 were a hydrogen atom, then the two diastereomers of the catalyst would be enantiomers, and the enantiomeric excess would be zero. ^{i}Pr is more similar than ^{t}Bu to hydrogen in terms of steric bulk, and because of this the energy difference between diastereomers is smaller for **C** than for **A**.

Ligand **D** is defined by $R_1 = R_2 = H$, $R_3 = {}^t$Bu. It is thus different from **A** in the nature of both the R_1 and R_2 substituents, which are replaced by hydrogens. More significantly, it differs from **B**, which has been shown above as fully equivalent to **A**, only in the R_1 substituent. Therefore, the study of **D** clarifies the role of this R_1 substituent. From the point of view of enantioselectivity, experimental data indicate that **D** is the least efficient ligand among the four considered here, with an associated enantiomeric excess of 46%.

From the computational point of view, the placement of a hydrogen atom in the R_1 position slightly simplifies the conformational complexity, because the different arrangements of the *tert*-butyl substituent in ligands **A** to **C** gave rise to the anty/syn labeling. In consequence, the four structures computed for **D** have one letter less in the label, and they are **D2ax1y1z1**, **D2ax1y1z2**, **D2bx1y1z2**, and **D2bx1y1z1**. Geometrical data are presented in Table 7, with energies collected in Table 4 and the drawing of the two most stable isomers in Figure 9. Geometrical parameters are in general similar to those for other ligands, confirming that the same overall reaction is taking place. **D** is in any case the ligand presenting the larger differences with respect to the other three, especially in the dihedral angles. For instance the dihedral angle O2−S1−S2−C9 has values of 0.6 ° and −11.2 ° for **A2aax1y1z1** and **A2aax1y1z2**, and the corresponding values for **D2ax1y1z1** and **D2ax1y1z2** are 15.9° and −14.4°, respectively. The general trend seems to be that in the case of **D**, the absolute values of the dihedral angles of the two transition states coming from the same diastereomeric form of the catalyst are much more similar, with differences of 1.5° at the most, while for ligands **A** to **C** differences of more than 10° are common.

This similarity of the two transition states associated to the same form of the catalyst is consistent with the relative energies, which are much closer to each other in **D**. The four computed structures are within a span of 0.7 kcal/mol, and the lowest energy structure leading to the **S** product is in this case **D2ax1y1z2**, coming from the **a** form of the catalyst, and with an energy of only 0.3 kcal/mol above **D2ax1y1z1**. This translates into a predicted enantiomeric excess of only 21%, smaller than the experimental value of 46%, but reproducing as always the experimental order of enantioselectivities among the ligands. The reduction in enantioselectivity of the overall reaction when replacing **A** by **D** is therefore associated to an intrinsic reduction of enantioselectivity for each diastereomeric form of the catalyst. Even if we could isolate a given form of the catalyst, either **D1a** or **D1b**, the selectivity would continue to be low.

The direct relationship between the steric bulk of R_1 and the intrinsic enantioselectivity of a given form of the catalyst has already been pointed out when discussing the stabilities of **A2aax1y1z1** and **A2aax1y1z2**. It can be easily understood by inspecting Figure 7 (transition states from the **A1a** catalyst), and the bottom part of Figure 9 (transition states from the **D1a** catalyst). The main reason for the energy difference of 2.4 kcal/mol between **A2aax1y1z1** and **A2aax1y1z2** (Figure 7) is the steric repulsion between the *tert*-butyl group at S1 and the *tert*-butyl group R_1. This interaction only exists in the **z2** isomer, on the right-hand side. In the **z1** isomer, on the left-hand side, the *tert*-butyl at S1 points in the opposite direction, largely reducing the steric strain. If we compare **D2ax1y1z1** and **D2ax1y1z2** (bottom of Figure 9), we see that the replacement of *tert*-butyl by hydrogen at the R_1 position eliminates the main cause of steric strain in the **z2** isomer, and thus of energy separation between the two transition states.

The fact that both diastereomeric forms of catalyst **D**, **a** and **b**, have such close energies is not directly explainable within the simple models presented above. It suggests some interplay between the R_1 and R_3 substituents. This has not been further explored because it does not bear a direct effect on the enantioselectivity of the reaction.

General Discussion

Our computational results on the vanadium-catalyzed oxidation of disulfides reproduce faithfully the trends observed experimentally upon modifications of the Schiff base ligand L (Figure 1). A high selectivity is obtained when the three substituents R_1, R_2, and R_3 are ^{t}Bu. The selectivity is unaffected by changes in ligand R_2, but it is very sensitive to changes in either R_1 or R_3. This is remarkable because R_1 and R_3 are quite

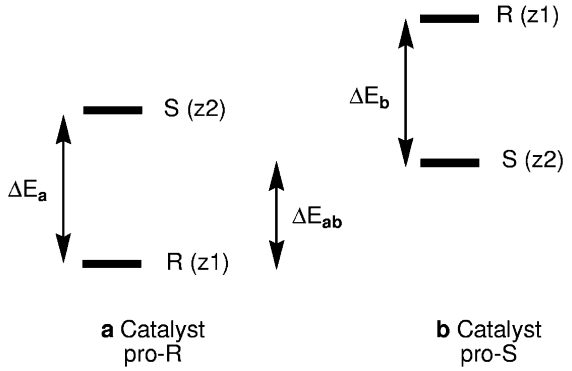

Figure 10. Energetic modulation of enantioselectivity.

far from each other, and it is not obvious how can both of them interact simultaneously with a relatively small substrate as ^{t}Bu−S−S−^{t}Bu. This behavior can be explained through the consideration of four of the many possible transition states that exist for the key step of this reaction, where the oxygen is transferred from a hydroperoxo ligand attached to vanadium to the disulfide.

In first place, one has to take into account the existence of two diastereomeric forms of the catalyst V(O)(L)(OOH), which we label arbitrarily as **a** and **b**. These two forms exist in equilibrium in solution because of the experimental method. The catalyst is prepared in situ through the mixture of a vanadium precursor $VO(acac)_2$, the enantiomerically pure ligand L, and hydrogen peroxide. This reaction creates a new chiral center at vanadium, which depending on how it is arranged with respect to the chiral ligand L produces one of two possible diastereomers. Both of them should be present in equilibrium in solution, their abundances depending on the relative energies.

Each of these diastereomeric forms of the catalyst can give rise to either the **R** or **S** enantiomer of the chiral ^{t}Bu−S−S(O)−^{t}Bu sulfoxide product. The enantioselectivity of the product depends on the absolute configuration at the sulfur atom carrying the oxygen, and this configuration is decided in the approach of the disulfide to the OOH hydroperoxo ligand of the catalyst. As a result, the problem of the enantioselectivity can be simplified in a first approach by considering the four possible transition states indicated in Figure 10. The idea is to take, for each diastereomer of the catalyst, the transition state with the lowest energy leading to each of the two possible products.

A first detail worth mentioning from Figure 10 is that while the **a** form of the catalyst is pro-**R**, leading preferably to the **R** product, the **b** form of the catalyst is pro-**S**. This has been the result in the four tested ligands, and it is probably a general behavior associated to the topological relationship between the **a** and **b** forms of the catalyst. On the other hand, Figure 10 can be applied to any sistem with this duality of catalyst forms, and it is mathematically characterized by the particular values of the ΔE_a, ΔE_b, and ΔE_{ab} parameters. The first two correspond to the energy differences between the two enantiomers within a given diastereomer of the catalyst, while the third one corresponds to the difference between the lowest energy transition states coming from each of the different diastereomeric catalysts.

What makes this model useful for the qualitative explanation of this particular reaction is the dependence of each of this ΔE parameters on the nature of the substituents R_1, R_2, and R_3 that has been determined from the calculations. The setting for ligand **A** is such that ΔE_a is larger than ΔE_{ab}, corresponding to what is shown in Figure 10. As a result, the minor **S** product comes essentially from the **b** form of the catalyst. The eventual steric bulk of R_2 has practically no effect on the enantioselectivity, as shown by the comparison between the results for ligands **A** and **B**. R_3 affects essentially ΔE_{ab}. When its steric bulk diminishes, as when going from **A** to **C**, the lowering of ΔE_{ab} brings a diminution of the enantiomeric excess, even if ΔE_a in fact increases slightly. R_1 in contrast affects essentially ΔE_a. As a result, for ligand **D**, the minor isomer **S** comes from the same catalytic form **a** as the major isomer **R** does. Ligand **D** also presents a reduction of ΔE_{ab}, but this is in fact less relevant to the overall selectivity.

Therefore, the dependence of the overall enantioselectivity on the nature of two different ligands can be explained by the presence of two different competition processes in this reaction. On one hand, there is the competition between the different transition states within a given catalyst, which is ruled by R_1. And on the other hand, there is the competition between the two different forms of the catalyst, which is ruled by R_3. The unexpected influence of distant substituents on the observed enantioselectivity is the simple manifestation of the presence of these two different types of competition.

Conclusions

The computational study with a QM/MM method on the oxidation of bis(*tert*)-butyl disulfide by V(O)(L)(OOH) (L = bulky Schiff base) explains satisfactorily the remarkable dependence of the selectivity of the reaction on the nature of the L ligand. Modifications in three different substituents at L, R_1, R_2, and R_3, have been considered. Two of them, R_1 and R_3 are found to be relevant, with the other one, R_2, having practically no effect, in good agreement with experimental data.

The systematic analysis of one particular combination of substituents, labeled as ligand **A** shows the great conformational complexity of the reaction process, with no less than eight possible structures for the catalyst and a much larger number of possible structures for the transition state in the key reaction step. The results on ligand **A** lead however to the characterization of a series of systematic trends, that largely simplify the work on other ligands. The study on ligands **B**, **C**, and **D** is thus reduced to the calculation of four selected structures without any significant reduction in the quality of the results. The computed values for the ee based on the analysis of these four pathways faithfully reproduces the experimental trends.

The unusual fact that two geometrically distant substituents can affect the selectivity of the same process is explained by the coexistence in the experimental conditions of two different forms of the catalyst, each of them leading preferentially to a different enantiomeric sulfoxide product. Substituent R_1 affects the selectivity within a given form of the catalyst, while substituent R_3 affects the selectivity between the two different forms of the catalyst. In this way, both of them affect the overall selectivity, but they do it through different mechanisms.

The reasonable reproduction by our QM/MM calculations of the experimental enantiomeric excess for the systems studied here suggests a good predictive ability of theoretical chemistry for this type of reactions. With this idea in mind, we are currently working in our Laboratory on the computational design of a more efficient catalyst for this process.

Acknowledgment. Financial support from the Spanish MCyT (project BQU2002-04110-CO2-02) and FEDER, the Catalan DURSI (project No. 2001SGR00179) and the ICIQ foundation is acknowledged. F.M. thanks also the support of DURSI. G.U. thanks the Spanish MCyT for funding through the "Ramón y Cajal" program.

Supporting Information Available: PDF file containing information (Cartesian coordinates, total energy, QM energy, MM energy) for the optimized geometries of the compounds mentioned with a label in the text: 8 conformers of catalyst **A1**, 12 conformers of transition states **A2a**, 5 conformers of transition states **A2b**, 4 conformers for each of transition states **B2**, **C2** and **D2**. This material is available free of charge via the Internet at http://pubs.acs.org.

JA0435384